Fully Automated Common Carotid Artery and Internal Jugular Vein Identification and Tracking Using B-Mode Ultrasound

David C. Wang*, Roberta Klatzky, Bing Wu, Gregory Weller, Allan R. Sampson, and George D. Stetten, *Associate Member, IEEE*

***Abstract*—We describe a fully automated ultrasound analysis system that tracks and identifies the common carotid artery (CCA) and the internal jugular vein (IJV). Our goal is to prevent inadvertent damage to the CCA when targeting the IJV for catheterization. The automated system starts by identifying and fitting ellipses to all the regions that look like major arteries or veins throughout each B-mode ultrasound image frame. The spokes ellipse algorithm described in this paper tracks these putative vessels and calculates their characteristics, which are then weighted and summed to identify the vessels. The optimum subset of characteristics and their weights were determined from a training set of 38 subjects, whose necks were scanned with a portable 10 MHz ultrasound system at 10 frames per second. Stepwise linear discriminant analysis (LDA) narrowed the characteristics to the five that best distinguish between the CCA and IJV. A paired version of Fisher's LDA was used to calculate the weights for each of the five parameters. Leave-one-out validation studies showed that the system could track and identify the CCA and IJV with 100% accuracy in this dataset.**

***Index Terms*—Biomedical acoustic imaging, biomedical engineering, biomedical image processing, blood vessels.**

I. Introduction

THE COMMON carotid artery (CCA) and the internal jugular vein (IJV) run side by side in the neck, one pair on the left and one on the right. The CCA carries oxygenated blood up to the head while the IJV drains deoxygenated blood down to the heart. The right IJV is a common entry site for intravascular procedures such as central catheter line placement, hemodynamic measurement, myocardial biopsy, and cardiac ablation. The right IJV is chosen because its path to the right atrium is straighter than that from the left IJV. Inadvertent CCA puncture while targeting the IJV is not uncommon (reported incidence of 2%–8% [1] [2]) and usually results in localized hematoma. The hematoma may enlarge rapidly if the patient is coagulopathic, or if a large puncture wound is produced by the introduction of the sheath itself into the CCA. Other potential negative consequences of CCA puncture include airway obstruction [3], pseudoaneurysm [4], arterio–venous fistula formation [5], retrograde aortic dissection [6], and cerebrovascular accident [7] with potentially fatal consequences.

The introduction of B-mode ultrasound to guide IJV access has decreased the arterial puncture incidence [8]. The direction and pattern of flow from color Doppler can further help distinguish arteries from veins. However, doctors generally hold the ultrasound transducer roughly perpendicular to the target vessels during vascular access, whereupon slight angular deviation may reverse the perceived direction of flow, making identification of the vessels ambiguous. Thus, color Doppler is generally only used during preoperative evaluation and not during the actual procedure.

We believe a fully automated vessel identification system operating in real time during the procedure could decrease the incidence of inadvertent CCA puncture and facilitate cannulation. We have developed such a system, in the form of software to be used in conjunction with a new method of ultrasound display, the sonic flashlight [9], which employs a half-silvered mirror to reflect the image directly within the patient. By analyzing the properties of the tracked objects, it should be possible to automatically classify and graphically mark each as an artery, vein, or other tissue type, with the markings being displayed by the sonic flashlight superimposed on the ultrasound image floating within the patient. Such markings could obviously be used with conventional ultrasound displays as well. In either case, it could help prevent the operator, especially the relative novice, from accidentally puncturing the CCA.

Due to the presence of speckle, the dependence of backscatter on beam orientation, and the attenuating effects of intervening structures, ultrasound is among the most difficult modalities for automated image analysis. A number of researchers have developed ultrasound segmentation techniques. The majority of effort has focused on the following clinical applications: echocardiography, breast ultrasound, transrectal ultrasound, intravascular ultrasound (IVUS), and ultrasound in obstetrics and gynecology [10]. Segmentation of the carotid artery using IVUS has been extensively studied [10]. These images are acquired

Manuscript received October 25, 2008; revised December 21, 2008. First published March 4, 2009; current version published June 10, 2009. This work was supported by the National Institutes of Health under Grant R01-EB000860 and Grant R01-HL074285-01. *Asterisk indicates corresponding author.*

*D. Wang is with the University of Pittsburgh School of Medicine, Pittsburgh, PA 15213 USA (e-mail: david@wangmd.com).

R. Klatzky and B. Wu are with the Department of Psychology, Carnegie Mellon University, Pittsburgh, PA 15213 USA (e-mail: klatzky@cmu.edu; bingwu@andrew.cmu.edu).

G. Weller is with the Department of Statistics, North Carolina State University, Raleigh, NC 27695 USA.

A. Sampson is with the Department of Statistics, University of Pittsburgh, Pittsburgh, PA 15261 USA.

G. Stetten is with the Department of Bioengineering, University of Pittsburgh, Pittsburgh, PA 15261 USA, and also with the Robotics Institute, Carnegie Mellon University, Pittsburgh, PA 15213 USA (e-mail: george@stetten.com).

Color versions of one or more of the figures in this paper are available online at http://ieeexplore.ieee.org.

Digital Object Identifier 10.1109/TBME.2009.2015576

from within the vessel using a catheter-based high-frequency (∼40 MHz) ultrasound probe, and provide an inherent central location within the lumen. In terms of image analysis, therefore, they are fundamentally different from our application. Transdermal ultrasound scans are typically performed at ∼8–10 MHz, and the location of the center of the lumen is unknown.

For transdermal vascular scans, Mao *et al.* used deformable models that incorporate knowledge about the shape and location of the desired feature [11]. In general, deformable models require careful initialization and tuning of parameters, and are difficult to implement in real time. A less computationally intensive algorithm is presented in [12] for the evaluation of deep vein thrombosis (DVT). A modified Star–Kalman algorithm, based on an elliptical model, is used to determine vessel contours. It includes a temporal Kalman filter to provide robust tracking of the vessel lumen. This is important for the DVT application, in which the entire length of a human leg is often scanned. For our clinical application, jugular vein cannulation, the ultrasound probe is held relatively stationary while a needle is guided into the vein. Thus, our tracking requirements are primarily in the temporal domain and need to deal mostly with changes in vessel size and shape, rather than location. Therefore, our seed points can be reliably determined simply by using the center of mass of the vessel as segmented in the previous time frame. Methods to identify anatomical targets in ultrasound images other than vascular structures have also been investigated. Drukker *et al.* researched the use of a radial gradient index filter to automatically detect lesions in breast ultrasound [13]. Ladak *et al.* developed automatic methods to segment the boundaries of the prostate [14]. Algorithms also exist for automatically locating instruments such as biopsy needles in an ultrasound image [15]. This list is not meant to be all-inclusive. Many researchers have applied image analysis to clinical ultrasound, but to our knowledge, our system is the first to automatically identify and differentiate in real time between the CCA and IJV.

We have approached the problem of identifying the CCA and IJV by creating a system that will simultaneously track multiple vessels under limited motion and provide statistical data for their identification. We scanned healthy subjects to determine statistically reliable vessel parameters and corresponding weights to optimally classify the vessels. The system operates in real time, enabling its potential introduction into ongoing clinical testing of the sonic flashlight [16] [17]. This paper expands upon preliminary results presented at Medical Image Computing and Computer-Assisted Intervention (MICCAI) 2006 [18] and describes the final system in detail.

We begin in Section II-A and II-B by introducing the spokes ellipse algorithm [18] for segmentation, tracking, and calculating the cross-sectional elliptical radii of each vessel. In Section II-C, we introduce the features that can potentially distinguish CCA from IJV. In Section III, we describe our dataset, methods to validate the data, and methods to calculate the variables described in Section II-C. In Section IV, we discuss the results and relate them to known vascular physiology. Finally, in Section V, we review our conclusions and directions for future work.

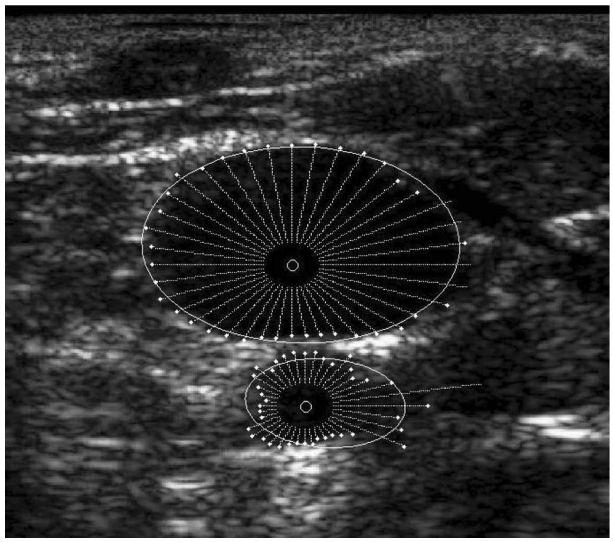

Fig. 1. *Spokes ellipse* algorithm applied to the IJV (top) and the CCA (bottom). Spokes grow until they reach a boundary (white dots) or a preset maximum length (lines without a dot). Ellipses are fit to the dots for each vessel. Algorithm runs in real time.

II. Background

A. Spokes Ellipse Algorithm

We have developed an efficient algorithm that tracks blood vessels in real time and simultaneously calculates their elliptical radii and cross-sectional area in each frame to be used for vessel classification.

The *spokes ellipse* algorithm outlines and tracks the vessel walls in a sequence of frames (Fig. 1), given an initialization process described in the next section. Much like the aforementioned "Star" algorithm, the *spokes ellipse* algorithm initially draws 30 radial lines emanating from a seed point. An intensity-threshold-based boundary detection algorithm searches for the most likely boundary along each spoke. Since the intensities of vascular walls are different at different depths, we use the 80th percentile intensity of all pixels at the same depth, for each frame, as the vascular boundary threshold for that particular depth. This threshold was determined by sampling pixels just outside the vessels and those just inside the vessels to determine the optimal cutoff value (data not shown). Spokes whose lengths are not within one standard deviation of the mean are eliminated. From the remaining spokes, an ellipse is fitted by a least squares method [10]. The cross-sectional area of the vessel is approximated by the area of the ellipse. The center of the ellipse is then used as the seed point for the spokes in the next frame. By recalculating the center of the vessel and its boundaries in each frame, the vessel can be tracked in real time, although sudden movement of the transducer may cause the tracking to be lost. This algorithm is run at least twice in each frame, since there are two vessels to track: the CCA and the IJV.

B. Spokes Ellipse Initialization

We explored three methods for initial identification of the blood vessels in the first frame: 1) manual initialization by an

expert; 2) automatic initialization with color Doppler; and 3) brute force testing of each pixel as a seed point for subsequent tracking and vessel identification. We describe them here, comparing their relative advantages and disadvantages.

1) An expert can manually initialize the *spokes ellipse* algorithm by tapping the CCA and IJV on a touch-sensitive screen to mark the approximate center of these two vessels. This is inherently a reliable process, given the relative ease with which most experts can identify large vessels in an ultrasound image. In a clinical setting, however, it is desirable not to require such a manual process, especially since it might have to be repeated each time tracking is lost.
2) Color Doppler, which detects blood flow, can be used to automatically initialize the ellipses. Although, as already mentioned, color Doppler may not reliably differentiate artery from vein when the transducer is perpendicular to the vessels, it does provide evidence of nonzero flow magnitude. However, due to the proximity of the CCA and IJV, color Doppler often cannot separate the two vessels into distinct clusters from which seed points can be derived.
3) The third option we explored to seed the tracking algorithm is a brute force approach in which the entire image (512×512 pixels) is blanketed with ellipse seed points spaced 10 pixels (horizontally and vertically) apart. Each ellipse then grows according to the *spokes ellipse* algorithm. Ellipses that do not fit properly (i.e., those with rms fitting error >0.07) are eliminated until only two properly fitting adjacent ellipses remain. Option 3) was used in the study described here, because it is very reliable and does not depend critically on transducer angle. It is also very fast, taking only a fraction of a second. In general, automated seeding of the CCA and IJV in this area of the neck (just above the clavicle) is not difficult, since there are rarely other ambiguous structures that can confuse our system.

C. Potential Features for Vessel Classification

A priori, we generated a set of 26 features that could be used for vessel classification. Table I lists these features along with their corresponding confidence intervals and p-values from the current data. The measures that form the basis for the feature set and the rationale for considering them are described here.

1) Ellipse Area: Since the blood volume is more dependent on gravity in the vein than in the artery, having the subject lie supine should increase the blood volume in the IJV.

2) Eccentricity: Being more compliant, the IJV may show a greater degree of eccentricity in elliptical shape, especially considering the pressure being applied by the ultrasound transducer.

3) Number of Spokes Retained and *Ellipse Fitting Error:* Since the spokes that grow beyond a boundary gap are eliminated, the number of spokes used and the ellipse fitting error are direct reflections of the completeness of the vascular boundary detected by ultrasound.

4) Depth of Ellipse Centers: Depth is a potentially important feature to distinguish the two vessels since the CCA generally lies deeper beneath the skin than the IJV. However, the relative locations of two vessels in the image depend on how the transducer is oriented and what portion of the neck is being scanned. One study has shown the IJV to be positioned completely lateral to the CCA in 8.7% of clinical scans [19]. Actually, doctors often prefer such lateral placement of the IJV because CCA puncture

TABLE I
95% CONFIDENCE INTERVAL AND p-VALUE FOR 26 PARAMETERS, DERIVED SEPARATELY FROM THE CCA AND IJV DATA

Parameter in each subject		Vessel	95% C. I.	P-value
Ellipse area (mm^2)	Mean	CCA	20.56 ± 1.49	<0.001
		IJV	39.87 ± 6.28	
	Standard deviation	CCA	2.985 ± 0.521	0.001
		IJV	4.197 ± 0.615	
	Lower 10th percentile	CCA	17.15 ± 1.38	<0.001
		IJV	34.54 ± 5.95	
	Upper 90th percentile	CCA	24.42 ± 1.91	<0.001
		IJV	45.11 ± 6.66	
Fourier transform	Heart rate (cpm)	CCA	61.08 ± 2.55	0.018
		IJV	62.69 ± 2.39	
	Magnitude at heart rate	CCA	20624 ± 2968	<0.001
		IJV	43579 ± 7983	
	Respiratory rate (cpm)	CCA	16.47 ± 1.36	0.054
		IJV	18.09 ± 1.17	
	Magnitude at respiratory rate	CCA	16857 ± 2660	<0.001
		IJV	27502 ± 4502	
	Slope of best fit line between 10 – 250 cpm	CCA	-15.49 ± 2.37	<0.001
		IJV	-35.50 ± 6.16	
	Phase difference	N/A	-1.65 ± 0.54	N/A
Eccentricity	Mean	CCA	0.66 ± 0.03	0.144
		IJV	0.68 ± 0.02	
	Standard deviation	CCA	0.09 ± 0.01	<0.001
		IJV	0.06 ± 0.01	
	Lower 10th percentile	CCA	0.54 ± 0.03	0.01
		IJV	0.60 ± 0.03	
	Upper 90th percentile	CCA	0.76 ± 0.02	0.333
		IJV	0.76 ± 0.02	
Number of spokes used	Mean	CCA	23.24 ± 0.55	<0.001
		IJV	24.26 ± 0.38	
	Standard deviation	CCA	1.61 ± 0.09	0.006
		IJV	1.44 ± 0.08	
	Lower 10th percentile	CCA	21.24 ± 0.58	<0.001
		IJV	22.39 ± 0.38	
	Upper 90th percentile	CCA	25.18 ± 0.54	0.002
		IJV	26.00 ± 0.44	
Ellipse fitting error (RMS)	Mean	CCA	0.02 ± 0.00	<0.001
		IJV	0.01 ± 0.00	
	Standard deviation	CCA	0.01 ± 0.00	<0.001
		IJV	0.01 ± 0.00	
	Lower 10th percentile	CCA	0.01 ± 0.00	<0.001
		IJV	0.01 ± 0.00	
	Upper 90th percentile	CCA	0.04 ± 0.00	<0.001
		IJV	0.02 ± 0.00	
Depth of ellipse centers (mm)	Mean	CCA	2.364 ± 0.126	<0.001
		IJV	1.583 ± 0.079	
	Standard deviation	CCA	0.0519 ± 0.0072	<0.001
		IJV	0.0336 ± 0.0059	
	Lower 10th percentile	CCA	2.302 ± 0.124	<0.001
		IJV	1.545 ± 0.078	
	Upper 90th percentile	CCA	2.431 ± 0.128	<0.001
		IJV	1.625 ± 0.081	

The last column shows the significance level (p) for a paired t-test comparing the CCA and IJV values across the subjects.

is less likely when it is not directly under the IJV. This reduces the potential usefulness of depth in vessel identification.

5) Properties of the Fourier Transform—Heart Rate, Respiratory Rate: Since the *spokes ellipse* algorithm allows for collection of information over several frames, we can compute temporal features of the vessels—frequencies and phase differences. The hemodynamics of the CCA and IJV differ in a consistent manner. The CCA experiences the highest blood pressure when the left ventricle contracts, causing a surge of blood to flow into the CCA through the aorta. The IJV experiences the highest blood pressure when the right atrium contracts, regurgitating blood to the IJV through the superior vena cava. Because the atria and ventricles do not contract simultaneously, the pulsations of the CCA and IJV are consistently out of phase in a given cardiac cycle.

By taking the Fourier transform of the temporal series of cross-sectional areas of each vessel, we can obtain a magnitude and phase at each frequency. The heart rate can be determined by identifying the frequency with the greatest magnitude in the physiologic range of 40–150 cycles per minute (cpm). Similarly, the respiratory rate can be determined as the frequency with greatest magnitude in the range 10–30 cpm. Recall that the Fourier transform $X(\omega)$ of a signal $x(t)$ can be represented in phasor notation as

$$X(\omega) = r(\omega)\, e^{j\theta(\omega)} \tag{1}$$

where $r(\omega) \geq 0$ is the magnitude and $-\pi < \theta(\omega) \leq \pi$ is the phase in the complex plane. Denoting the Fourier transforms of the IJV and CCA cross-sectional areas, respectively, as $J(\omega)$ and $C(\omega)$, the phase difference $Q(\omega)$ between the CCA and IJV can be found from their ratio, normalized by their relative magnitudes

$$Q(\omega) = \frac{r_J(\omega)}{r_C(\omega)} \frac{C(\omega)}{J(\omega)} = e^{j(\theta_C(\omega) - \theta_J(\omega))}. \tag{2}$$

This yields a unit phasor, the phase of which is the difference between the phases of the CCA and IJV at frequency ω

$$\Delta\theta(\omega) = \theta_C(\omega) - \theta_J(\omega). \tag{3}$$

Thus,

$$\Delta\theta(\omega) = \arctan \frac{\mathrm{Im}\{Q(\omega)\}}{\mathrm{Re}\{Q(\omega)\}}. \tag{4}$$

Since we have a sampled Fourier transform, individual phase samples may or may not represent a consistent phase difference, so we convolve over a narrow band in the frequency domain with a normalized Gaussian smoothing filter $G(\omega, \sigma)$ as follows:

$$\Delta\tilde{\theta}(\omega) = \arctan \frac{\mathrm{Im}\{G(\omega,\sigma) * Q(\omega)\}}{\mathrm{Re}\{G(\omega,\sigma) * Q(\omega)\}} \tag{5}$$

with σ set empirically to three samples or 2.5 cpm in the Fourier frequency domain, given a frame rate of 10 frames per second (fps) over 512 samples. Note that convolution can be applied to the complex number $Q(\omega)$ by applying it independently to the real and imaginary parts. A measure of phase consistency for this smoothed phase difference is

$$\alpha(\omega) = |G(\omega,\sigma) * Q(\omega)|. \tag{6}$$

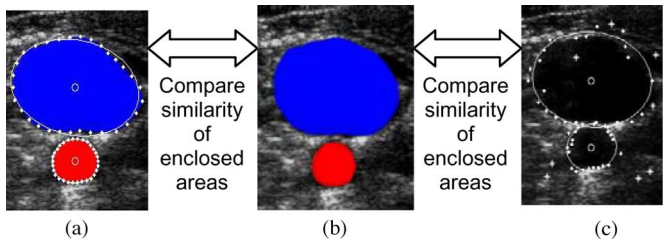

Fig. 2. Similarity between (b) the area of the *expert* tracing and (a) the ellipse fit to the *expert* tracing as well as (c) the algorithm defined ellipse.

Random phase differences in individual samples of the Fourier transform due to noise tend to cancel upon convolution with the Gaussian, yielding a value of $\alpha(\omega)$ near 0, whereas a consistent phase shift over consecutive frequency samples of the Fourier transform yields a value near 1.

III. Method

A. Data Acquisition

We recruited 42 healthy volunteers ages 20–51. The volunteers were asked to lie supine with their heads turned to the left. The right sides of their necks were scanned by a radiologist-trained senior medical student, hereafter referred to as the "*expert*." A commercially available scanner with a 10-MHz US probe (Terason 2000; Teratech, Burlington, MA) was used in the standard manner, using the standard vascular preset to adjust for intensity attenuation. A series of uncompressed, 512×512 pixel, digitized images, with pixel dimensions of 0.1×0.1 mm^2, was recorded by the ultrasound scanner at 10 fps for 120 s. Heart rates were measured by the *expert using palpation* before and after the scan, and the average used to estimate heart rate during the scan. Four subjects with collapsed IJVs, as determined by the *expert*, were excluded from the study. The *spokes ellipse* algorithm was applied to all frames collected from each of the 38 remaining subjects, and the first 512 continuously tracked frames were used in our analysis. (We used 512 frames because a power of 2 is required for the fast Fourier transform in our algorithm, and because twice that many were not needed.)

B. Validation of the Spokes Ellipse Algorithm

The *spokes ellipse* algorithm requires two assumptions: 1) the vessels' cross sections are elliptical and 2) the algorithm-drawn ellipses are similar to the manual traces of the lumen drawn by the *expert*. We define the similarity between two areas as

$$\frac{2 \times (\text{Area 1} \cap \text{Area 2})}{\text{Area 1} + \text{Area 2}} \times 100. \tag{7}$$

A perfect similarity would thus have a value of 100% [21].

The *expert* segmented five random image frames per subject. We compared the manual segmentations against those derived from the *spokes ellipse* algorithm (Fig. 2). We then tested the similarity between the area of the *expert* traced area itself and: 1) the ellipse fit to the *expert* tracing and 2) the algorithm defined ellipse, to test assumptions 1 and 2, respectively.

C. Vessel Property Calculations

For each subject and for each vessel, cross-sectional areas were calculated and the Fourier transform applied. This allowed for determination of the heart rate and respiratory rate. We then calculated the phase and magnitude in the frequency domain at the heart rate for each vessel. As described in Section II, this permitted calculation of phase shift and phase consistency.

In general, an artery has a thicker muscular layer than a vein of similar diameter. Thus, the artery is stiffer while the vein is more compliant. A stiffer material emphasizes high frequencies and attenuates low frequencies. A compliant material does the opposite. We analyzed this phenomenon by calculating the slope of the linear regression that best fit the Fourier transforms from 10 to 250 cpm.

Since the vein is more compliant and contains blood at a lower pressure, it would seem less likely to assume a circular shape than an artery. We calculated the eccentricity of the two vessels as

$$\text{eccentricity} = \sqrt{1 - \frac{b^2}{a^2}} \tag{8}$$

where a is the semimajor axis and b is the semiminor axis.

We also looked at whether the IJV is consistently closer to the skin than the CCA, as well as their absolute depths (measured by distance between the centers of each vessel to the skin). In addition, we considered the number of retained spokes and the magnitude of the ellipse fitting error, as already described.

D. Vessel Classification Using Vessel Properties

The vessel classification problem can be reduced to ordering the elements of a set: {CCA, IJV}. Given a pair of vessels with feature vectors $(\mathbf{v}_{ki}, \mathbf{v}_{(1-k)i})$, where k equals 0 or 1, in a series of tracked ultrasound images from a subject i, we wish to determine k such that $\mathbf{v}_{0i} = \text{CCA}$ and $\mathbf{v}_{1i} = \text{IJV}$. This is equivalent to determining the order in which the vessels were given where {CCA, IJV} is group $k = 0$ and {IJV, CCA} is group $k = 1$.

We represent the m characteristics of each vessel for each subject i by the m-dimensional vectors

$$\begin{aligned} \mathbf{v_{ki}} &= (v_{ki1},\ v_{ki2}, \ldots,\ v_{kim}) \\ \mathbf{v_{(1-k)i}} &= (v_{(1-k)i1},\ v_{(1-k)i2}, \ldots,\ v_{(1-k)im}). \end{aligned} \tag{9}$$

The difference $\mathbf{d}$ is calculated between each pair of vessels for each subject i in both directions

$$\begin{aligned} \mathbf{d}_{ki} &= \mathbf{v}_{ki} - \mathbf{v}_{(1-k)i} \\ \mathbf{d}_{(1-k)i} &= \mathbf{v}_{(1-k)i} - \mathbf{v}_{ki}. \end{aligned} \tag{10}$$

Note that phase difference at the heart rate is a property between two vessels and not of either vessel alone. It is already in the form of $\mathbf{v}_{0i} - \mathbf{v}_{1i}$ for $\mathbf{d}_{0i}$, so we can simply take its negative to obtain $\mathbf{v}_{1i} - \mathbf{v}_{0i}$ for $\mathbf{d}_{1i}$.

With this representation of the parameters, our goal is to find a set of weights $\mathbf{w} = (w_1, w_2, \ldots, w_m)$ such that $\mathbf{w} \cdot \mathbf{d}_{0i}$ is positive and $\mathbf{w} \cdot \mathbf{d}_{1i}$ is negative. In other words, if $\mathbf{w} \cdot \mathbf{d}_{ki}$ is positive, then the first and second given vessels are most likely to be CCA and IJV, respectively. If not, then they are most likely to be IJV and CCA, respectively, instead. The weights can be found through Fisher's linear discriminant analysis (LDA) [22].

However, the large parameter space (a total of 26 parameters are computed by our algorithm, as will be described later) may result in overfitting. In overfit models, variables that truly do have the power to predict the correct group are somewhat marginalized in their importance, and the predicting power of the "weak" variables tends to be greatly overexaggerated. Therefore, we need to reduce the dimensionality of the parameter space.

To identify the set of the most differentiating parameters based on the vessel differences, we used forward stepwise LDA (SLDA) as implemented in the statistical package Statistical Package for the Social Sciences (SPSS, Chicago, IL) with Wilks' lambda as the measure of significance. Small Wilks' lambda values indicate those difference variables with high discriminatory value between the groups of interest, $k = 0$ versus $k = 1$. SLDA works by starting with the null set of variables and adding one variable at a time: the variable that most reduces the Wilks's lambda of the set given the presence of the previously selected variables. The addition of variables continues until no more significant variables can be identified. This reduces the dimensionality of the parameter space on which Fisher's LDA subsequently operates to determine $\mathbf{w}$. A leave-one-subject-out analysis was performed to validate the SLDA's parameter selection as well as the Fisher's LDA calculation of $\mathbf{w}$.

IV. Results

A. Analysis of Tracking

The *expert* verified that the algorithm, using the brute force seeding method, successfully tracked the vessels in the first 512 frames of 38 subjects. The 512 frames from each of the 38 subjects were used to calculate the vessel parameters.

Loss of tracking occurred in four subjects after their first 512 frames (although those first 512 frames were still used in the study). An analysis of the tracking loss provided some interesting observations. The vessels in these frames are either small or have incomplete vascular borders on ultrasound. This was reflected in abnormal values observed in at least one of the following parameters: 1) ellipse fitting error greater than 0.07; 2) ellipse area < 500 pixels^2; 3) fewer than ten eligible spokes; or 4) the two ellipses separated by more than 10 pixels. Although this observation is only anecdotal given the present dataset, we envision the ability, eventually, to develop an automated system for detecting loss of tracking based on a combination of such parameters.

B. Validation of the Spokes Ellipse Algorithm

As shown in Table II, among the 190 sampled images (38 subjects $\times 5$ random frames from each), there was a high similarity between the manual tracings of the lumen and the ellipses fitted to these tracings, indicating that the cross-sectional areas of the vessels were reasonably elliptical (assumption 1). The similarity between ellipses fit by the algorithm and the

TABLE II
SIMILARITY BETWEEN VESSEL CROSS-SECTIONAL AREA ESTIMATIONS (THE RANGES REPRESENT 95% CONFIDENCE INTERVAL)

	Manual tracing of the lumen vs. ellipses fit to those tracings	Manual tracing of the lumen vs. ellipses fit by our algorithm
CCA	96.8 ± 1.2%	82.6 ± 7.0%
IJV	93.8 ± 3.1%	86.9 ± 6.1%

manual tracings was also high, indicating that the algorithm had basically extracted the same area as the *expert* (assumption 2).

C. Vessel Feature Comparisons

Having validated the *spokes ellipse* algorithm for basic segmentation, we next tested its use in generating features for vessel classification by comparing the values of features generated by the algorithm between the CCA and IJV. Table I lists the confidence intervals and p-values for these comparisons. Features with significant differences are candidates for distinguishing between the two vessels, although the size of the difference should also be considered.

1) Ellipse Area: As expected from relative blood volume, ellipse cross-sectional areas of the IJV were significantly larger than those of the CCA.

2) Eccentricity: It was expected that, being more compliant, the IJV would show a greater degree of eccentricity. However, the respective means of eccentricity for the CCA and IJV were 0.66 ± 0.03 and 0.68 ± 0.02, a nonsignificant difference. Eccentricity is inherently dependent on the angle between image plane and direction of the vessel, so that even circular vessels can appear eccentric when scanned at an angle. The slightly higher standard deviation of eccentricity for the CCA also conflicts with the expectation that the IJV would show a greater variation in eccentricity over time. Thus, eccentricity is suspect as a viable differentiating factor.

3) Number of Spokes Retained and Ellipse Fitting Error: The data showed that the CCA retained significantly fewer spokes than the IJV. This means the boundary of the CCA is more likely to be ill-defined than the IJV. A direct consequence is that the ellipse fitting error is also greater when fitting ellipses to the CCA compared to the IJV.

4) Depth of Ellipse Centers: The CCA was found to be significantly deeper beneath the skin than the IJV, as expected. However, we did not further consider depth, for reasons given before.

5) Fourier Transform: The changes over time for the cross-sectional areas of the CCA and IJV in a typical subject are shown in Fig. 3, and their Fourier transforms are shown in Fig. 4(a) and (b). The heart rate in this subject corresponds to the peak in magnitude around 60 cpm and is consistent with that determined by palpation during the scan. Although the heart rates extracted from the transform for each vessel should theoretically be identical, and the difference is small, it is actually statistically reliable ($p < 0.05$). This may be due to the shapes of the magnitude peaks in the frequency spectrum given that a simple maximum was used.

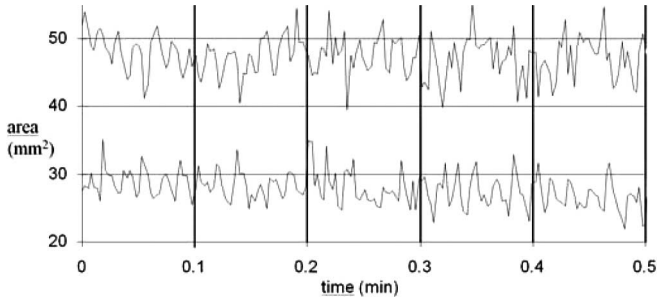

Fig. 3. Time series of the cross-sectional areas of the IJV (top) and the CCA (bottom) in a typical subject (subject #33) over a period of 30 s. Note the peaks and troughs appear generally out of phase.

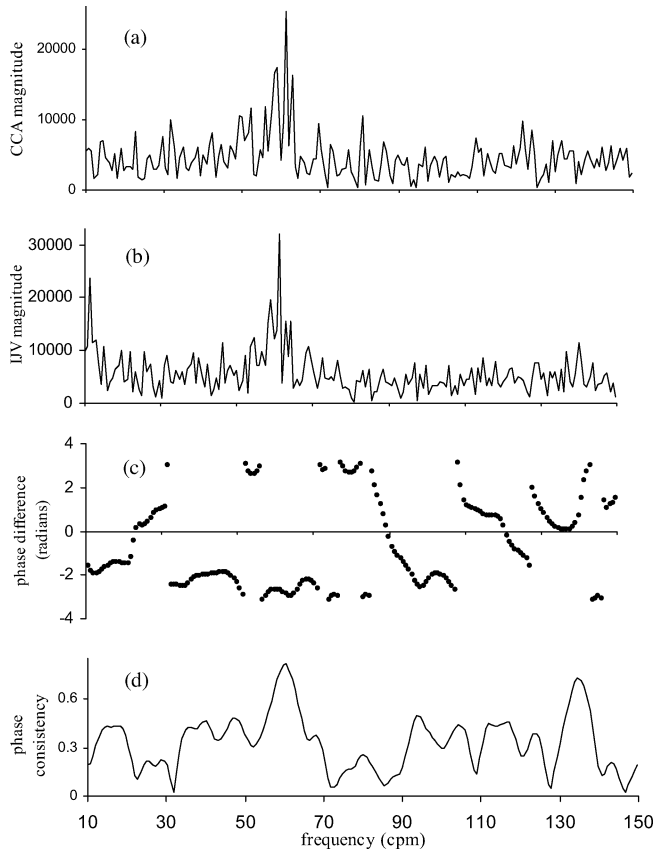

Fig. 4. Parameters of subject #33 in frequency domain. (a) Lower frequency spectrum of Fourier transform of the time series of CCA cross-sectional areas. (b) Fourier transform of the time series of IJV cross-sectional areas. (c) Phase difference between CCA and IJV. (d) Phase consistency between CCA and IJV.

The respiratory rates extracted from the two Fourier transforms did not differ significantly, as expected.

The slope of the lower frequencies (10–250 cpm) in the Fourier transform of the IJV (-35.50 ± 6.16) was significantly more negative than that of the CCA (-15.49 ± 2.37), with a p-value <0.05. This is consistent with the IJV being more compliant than the CCA, and thus attenuating the higher frequencies. This also explains the higher magnitude of the IJV Fourier transform at the heart rate and respiratory rate, which are typically in the lower half (10–130 cpm) of the spectrum.

TABLE III
STEPWISE WILKS' LAMBDA STATISTICS AND STANDARDIZED CANONICAL DISCRIMINANT FUNCTION COEFFICIENTS (w_i)

Step	Variable entered at each step	Wilks' Lambda	w_i
1	Difference in slope of Fourier transform's lower frequency spectrum trend line	0.479	0.674
2	Phase shift between the vessels	0.264	-0.755
3	Difference in mean ellipse fitting error between the vessels	0.174	-1.793
4	Difference in heart rate between the vessels	0.133	1.067
5	Difference in the upper 90th percentile ellipse fitting error between the vessels	0.126	1.057

6) Phase Difference and Consistency From Fourier Transform: Phase differences show high consistencies (not shown in Table I) around the frequency of the heart rate. This phase difference at the heart rate has a 95% confidence interval of -1.65 ± 0.54 rad. If we had reversed the CCA and IJV in the calculation of phase difference, the 95% confidence interval would simply be the negative, i.e., 1.65 ± 0.54 rad. Since these confidence intervals include neither 0 nor π, it appears that phase difference can be reliably used to differentiate between the CCA and the IJV. For the particular patient shown in Fig. 4, near the heart rate of 60 cpm, the phase difference is 2.2 rad and the phase consistency is 0.9.

D. Vessel Classification Using Vessel Features

By not considering the depth difference between CCA and IJV, we reduced the number of parameters for each subject from 26 to 22. We used SLDA to determine the best predictor variables and also their weights for this dataset (Table III), further reducing the effective parameter space from 22 to 5. The classification of each pair of observed blood vessels was done by calculating the dot product of $\mathbf{w}$ and $\mathbf{d}_{ki}$. Pairs of blood vessels were classified as either $\{$CCA, IJV$\}$ (class $k = 0$) or $\{$IJV, CCA$\}$ (class $k = 1$). The results are shown in Fig. 5. Data points representing class $k = 0$ are diamond shaped while those representing class $k = 1$ are circles.

The classification method was validated using leave-one-subject-out analyses, in which each subject was used for testing while the remaining 37 subjects were used for training. It turns out that the same five variables were selected in each of the 37 sets. These results are represented by $+$'s for class 0 and X's for class 1. The two permutation classes are separated completely by the zero line and are mirror images of each other, a consequence of their underlying parameters being negatives of each other. The *expert* determined that the vessels were correctly classified in all iterations. They appear to cluster around 0.26 and -0.26, respectively. The leave-one-subject-out studies show a greater degree of variance from the cluster centroids, as would be expected, but they are still separated completely by the zero line. The results demonstrate that our method can automatically and accurately distinguish between the CCA and IJV in B-mode ultrasound.

A histogram (Fig. 6) shows that the LDA of the five parameters separates the two permutation classes into two well-defined, approximately normally distributed, mirror image clusters in leave-one-out studies. The dot products for all the $\{$CCA, IJV$\}$ permutations are above 0 while the $\{$IJV, CCA$\}$ permutations are below 0.

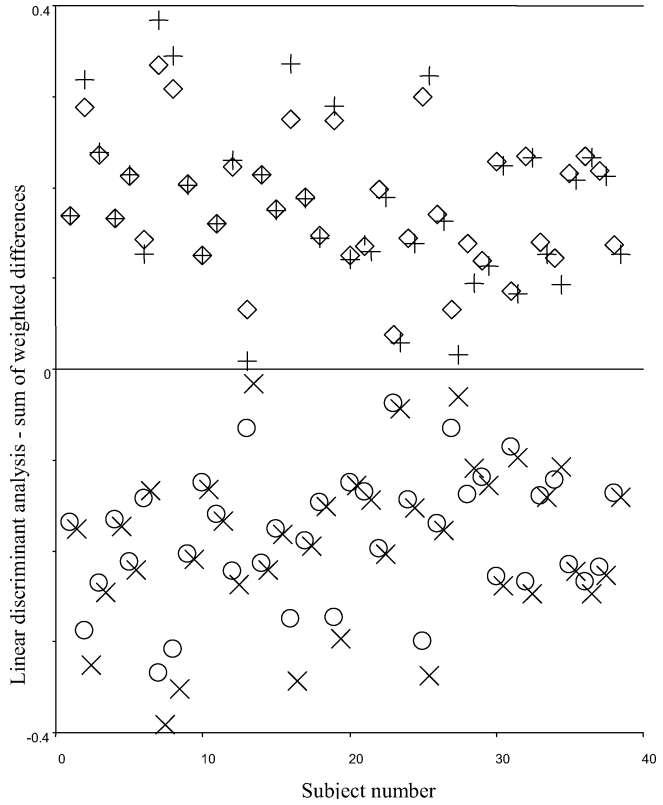

Fig. 5. Fisher's LDA based on five selected variables applied to all 38 subjects. Diamonds represent the permutation $\{$CCA, IJV$\}$ whose parameters are weighed and summed based on weights derived from the entire 38-subject training set. Circles represent the other permutation: $\{$IJV, CCA$\}$. $+$'s represent the permutation $\{$CCA, IJV$\}$ from each subject whose parameters are weighed and summed based on weights derived from the other 37 subjects. X's represent the other permutation.

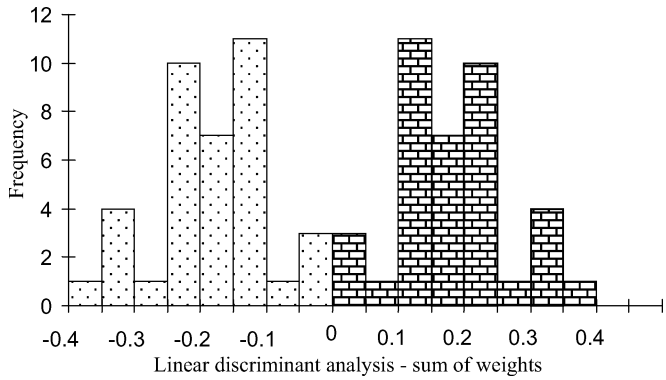

Fig. 6. Frequency distribution of the weighted sum of the five parameters on each subject using weights derived from Fisher's LDA of the other 37 subjects. The dotted histograms represent the $\{$IJV, CCA$\}$ permutations while the brick textured histograms represent the $\{$CCA, IJV$\}$ permutations.

V. CONCLUSION

We have shown in each of our 38 subjects (after excluding 4 with collapsed IJVs, who would not normally be candidates for

catheter insertion) that the spokes ellipse algorithm maintained tracking for at least 51 s (512 continuous frames) during the 120-s ultrasound scans. Although the CCA and IJV both pulsate, we have verified that the differences in depth of the vessels alone can distinguish between the vessels. However, in clinical situations where doctors often seek probe positions that orient the vessels side by side, a combination of other intrinsic vessel properties can be used to distinguish reliably between the vessels: the slopes of the Fourier transforms, phase shift between the vessels, heart rate as determined from the Fourier transforms, and the mean and upper 90th percentile ellipse fitting error.

A real-time system has been constructed into a clinical ultrasound machine that examines the image frames, determines the locations of two candidate vessels by brute force ellipse fitting, fits ellipses using the *spokes ellipse* algorithm, and calculates the relevant parameters. In just a few seconds, after sufficient frames have been acquired to perform a Fourier transform, the system marks the CCA red and the IJV blue. In the indeterminate case (if the data point is too close to the zero line in Fig. 6), both are marked green. The entire calculation is performed on our laptop system well within 0.1 s, allowing a 10-fps image acquisition rate. The graphically overlaid markers are projected within the patient along with the ultrasound image by the sonic flashlight. After initialization, the system tracks in real time by using a sliding window of previous frames. Our results, although limited to healthy subjects, show that the system can reliably detect and label the CCA and IJV on this population. Future work includes extending the methods we used to identify the vessels to detect patterns of pathology, based on ultrasound scans of the CCA and IJV.

ACKNOWLEDGMENT

The author would like to thank the members of the Visualization and Image Analysis Laboratory at University of Pittsburgh for volunteering for ultrasound scans.

REFERENCES

[1] M. J. Davies, K. D. Cronin, and C. M. Domaingue, "Pulmonary artery catheterization: An assessment of risks and benefits in 220 surgical patients," *Anaesth. Intensive Care*, vol. 10, no. 1, pp. 9–14, 1982.

[2] C. Patel, V. Laboy, B. Venus, M. Mathru, and D. Wier, "Acute complications of pulmonary artery catheter insertion in critically ill patients," *Crit. Care Med.*, vol. 14, no. 3, pp. 195–197, Mar. 1986.

[3] J. S. W. Kua and I. K. S. Tan, "Airway obstruction following internal jugular vein cannulation," *Anaesthesia*, vol. 52, pp. 776–780, 1997.

[4] H. Aoki, T. Mizobe, S. Nozuchi, T. Hatanaka, and Y. Tanaka, "Vertebral artery pseudoaneurysm: A rare complication of internal jugular vein catheterization," *Anesth. Analg.*, vol. 75, pp. 296–298, 1992.

[5] F. Gobeil, P. Couture, D. Girard, and R. Plante, "Carotid artery-internal jugular fistula: Another complication following pulmonary artery catheterization via the internal jugular venous route," *Anesthesiology*, vol. 80, pp. 23–232, 1994.

[6] R. M. Applebaum, M. A. Adelman, M. S. Kanschuger, G. Jacobowitz, and I. Kronzon, "Transesophageal echocardiographic identification of a retrograde dissection of the ascending aorta caused by inadvertent cannulation of the common carotid artery," *J. Amer. Soc. Echocardiogr.*, vol. 10, no. 7, pp. 749–751, Sep. 1997.

[7] N. A. Zaidi, M. Khan, H. I. Naqvi, and R. S. Kamal, "Cerebral infarct following central venous cannulation," *Anaesthesia*, vol. 53, pp. 186–191, Feb. 1998.

[8] B. G. Denys, B. F. Uretsky, and P. S. Reddy, "Ultrasound-assisted cannulation of the internal jugular vein: A prospective comparison to the external landmark-guided technique," *Circulation*, vol. 87, pp. 1557–1562, 1993.

[9] G. D. Stetten and V. Chib, "Overlaying ultrasound images on direct vision," *J. Ultrasound Med.*, vol. 20, no. 3, pp. 235–240, 2001.

[10] J. A. Noble and D. Boukerroui, "Ultrasound image segmentation: A survey," *IEEE Trans. Med. Imag.*, vol. 25, no. 8, pp. 987–1010, Aug. 2006.

[11] F. Mao, J. Gill, D. Downey, and A. Fenster, "Segmentation of carotid artery in ultrasound images: Method development and evaluation technique," *Med. Phys.*, vol. 27, no. 8, pp. 1961–1970, 2000.

[12] J. Guerrero, S. E. Salcudean, J. A. McEwen, B. A. Masri, and S. Nicolaou, "Real-time vessel segmentation and tracking for ultrasound imaging applications," *IEEE Trans. Med. Imag.*, vol. 26, no. 8, pp. 1079–1090, Aug. 2007.

[13] K. Drukker, M. L. Giger, K. Horsch, M. A. Kupinski, C. J. Vyborny, and E. B. Mendelson, "Computerized lesion detection on breast ultrasound," *Med. Phys.*, vol. 29, no. 7, pp. 1438–1446, Jul. 2002.

[14] H. M. Ladak, F. Mao, Y. Wang, D. B. Downey, D. A. Steinman, and A. Fenster, "Prostate boundary segmentation from 2D ultrasound images," *Med. Phys.*, vol. 27, no. 8, pp. 1777–1788, Aug. 2000.

[15] K. J. Draper, C. C. Blake, L. Gowman, D. B. Downey, and A. Fenster, "An algorithm for automatic needle localization in ultrasound-guided breast biopsies," *Med. Phys.*, vol. 27, no. 8, pp. 1971–1979, Aug. 2000.

[16] W. Chang, N. Amesur, D. Wang, A. Zajko, and G. Stetten, "First clinical trial of the sonic flashlight—Guiding placement of peripherally inserted central catheters," in *Proc. 2005 Meeting Radiol. Soc. North Amer.*, Chicago, IL, Nov., pp. SSJ03–SSJ02.

[17] D. Wang, N. Amesur, G. Shukla, A. Bayless, D. Weiser, A. Scharl, D. Mockel, C. Banks, B. Mandella, R. Klatzky, and G. stetten, "Peripherally inserted central catheter placement with the sonic flashlight: Initial clinical trial by nurses," *J. Ultrasound Med.*, vol. 28, pp. 651–656, 2009.

[18] D. Wang, R. Klatzky, N. Amesur, and G. Stetten, "Carotid artery and jugular vein tracking and differentiation using spatiotemporal analysis," in *Proc. Med. Image Comput. Comput.-Assisted Intervention (MICCAI 2006)* (Lecture Notes Comput. Sci.), vol.4190, pp. 654–661.

[19] M. Pilu, A. Fitzgibbon, and R. Fisher, "Ellipse-specific direct least-square fitting," in *Proc. IEEE Int. Conf. Image Process.* Los Alamitos, CA: IEEE Comput. Soc. Press, 1996, vol.3, pp.599–602.

[20] C. A. Troianos, R. J. Kuwik, J. R. Pasqual, A. J. Lim, and D. P. Odasso, "Internal jugular vein and carotid artery anatomic relation as determined by ultrasonography," *Anesthesiology*, vol. 85, pp. 43–48, 1996.

[21] A. Zijdenbos, B. Dawant, and R. Marjolin, "Morphometric analysis of white matter lesions in MR images: Methods and validation," *IEEE Trans. Med. Imag.*, vol. 13, no. 4, pp. 716–724, Dec. 1994.

[22] D. Poxton, J. Graham, and J. F. W. Deakin, "Detecting asymmetries in hippocampal shape and receptor distribution using statistical appearance models and linear discriminant analysis," in *Proc. Br. Mach. Vis. Conf.*, 1998, pp. 525–534.

David C. Wang received the B.A. and M. Eng. degrees in computer science from Cornell University, Ithaca, NY, the Ph.D. degree in biomedical engineering from Carnegie Mellon University, Pittsburgh, PA, and the M.D. degree from the University of Pittsburgh School of Medicine, Pittsburgh.

He is a radiology resident at the University of Pittsburgh Medical Center. His current research interests include image guidance for interventional procedures as well as pattern recognition in medical images.

Roberta Klatzky received the Ph.D. degree in psychology from Stanford University, Stanford, CA.

She is a Professor of psychology and human–computer interaction at Carnegie Mellon University, Pittsburgh, PA. Her current research interests include human perception and cognition. She was engaged in research on perceptually guided action, navigation under visual and nonvisual guidance, and haptic and visual object recognition. Her work has been applied to navigation aids for the blind, haptic interfaces, exploratory robotics, image-guided surgery, and virtual environments.

Bing Wu received the M.S. degree in neurobiology from Shanghai Institute of Physiology, Chinese Academy of Sciences, Shanghai, China, in 1997, and the M.S. degree in computer science and the Ph.D. degree in experimental psychology from the University of Louisville, Louisville, KY, in 2002 and 2004.

He is currently a Postdoctoral Researcher in the Department of Psychology, Carnegie Mellon University, Pittsburgh, PA. His current research interests include perception of depth in the real, augmented, and virtual environments. He is the author or coauthor of 34 journal and conference publications.

Gregory Weller received the B.S. and M.A. degrees in statistics from the University of Pittsburgh, Pittsburgh, PA, in 2006 and 2007, respectively. He is currently working toward the Ph.D. degree in statistics at the North Carolina State University, Raleigh.

Allan R. Sampson received the Ph.D. degree in statistics from Stanford University, Stanford, CA, in 1970.

He is currently a Professor in the Department of Statistics, University of Pittsburgh, Pittsburgh, PA, where he also holds a secondary appointment in the Department of Biostatistics.

Prof. Sampson is a Fellow of the American Statistical Association and the Institute of Mathematical Statistics.

George D. Stetten (A'90) received the M.S. degree in biology from New York University, New York, in 1986, the M.D. degree from the State University of New York, Syracuse, in 1991, and the Ph.D. degree in biomedical engineering from the University of North Carolina at Chapel Hill, Chapel Hill, in 1999.

He is currently a Professor of bioengineering at the University of Pittsburgh, Pittsburgh, PA. He is also a Research Professor of robotics at Carnegie Mellon University, Pittsburgh.